Single cysteine adsorption on Au(110): A first-principles study

B. Höffling, F. Ortmann, K. Hannewald, and F. Bechstedt
European Theoretical Spectroscopy Facility and Institut für Festkörpertheorie und -optik, Friedrich-Schiller-Universität Jena, Max-Wien-Platz 1, 07743 Jena, Germany

(Received 11 August 2009; revised manuscript received 12 November 2009; published 12 January 2010)

The single-molecule adsorption of cysteine on the Au(110) surface is investigated by means of density-functional theory. The amino-gold and thiolate-gold bonds are studied separately to assess their relative contribution to the molecule-substrate bond. We analyze the bonding strength, electron redistribution, and changes in the density of states for the isolated bonds of these functional groups to the surface and for simultaneous bonding via both groups. Adsorbate-substrate geometries are obtained from total-energy minimizations. Flat adsorption configurations with S-Au at an off-bridge site and NH_2-Au at an off-top site are found to be energetically favored.

DOI: 10.1103/PhysRevB.81.045407 PACS number(s): 68.43.Bc, 68.43.Fg, 73.20.Hb, 82.65.+r

I. INTRODUCTION

The adsorption of organic molecules on crystal surfaces has attracted much interest in recent years. Special attention has been devoted to metal/organic interfaces,[1–10] which are of particular interest for the development of molecular electronics.[11–14] Recent findings about work-function change upon adsorption cannot be explained from the ionization potential of the molecule and the metal work function but require a detailed analysis of the adsorbate-substrate-interaction including the formation of interface dipoles and the pushback of surface electrons known as pillow effect.[2] Moreover, each molecule may have more than one preferred mode of interaction with a substrate. The existence of different functional groups leads to numerous possible configurations for the organic functionalization of the substrates, each of which is characterized by a unique electronic signature as evident from single-molecule conductance experiments.[15]

A prototypical example for the adsorption of biomolecules and chemical or electrical functionalization of surfaces is the interaction of the amino-acid cysteine $HS\text{-}CH_2\text{-}CH(NH_2)\text{-}COOH$ with gold surfaces.[16–25] Since cysteine not only contains the -SH thiol head group, which establishes strong bonds through its deprotonized sulfur atom but also the NH_2 amino group, its adsorption behavior is rather complex. Recent studies were mainly focused on the Au(111) surface while much less information can be found for the Au(110) surface. Scanning-tunneling microscopy (STM) investigations of cysteine deposited on the Au(111) surface revealed highly ordered networklike clusters[16–18] as well as a variety of other ordered structures, depending on temperature and coverage.[18] Density-functional theory (DFT) calculations of cysteine adsorption on Au(111) (Ref. 26) have shown flat adsorption geometries to be energetically favored over upright configurations, taking advantage of both the amino and the thiolate bonds. Sulfur-substrate interaction via a deprotonized thiolate group has been shown to create stronger bonds than dimer disulfide bonding.[27]

Recent STM investigations have discovered a variety of well-ordered structures of cysteine on the Au(110)-(1×2) surface, such as homochirally adsorbed dimers,[19] unidirectional molecular rows,[20] and large homochiral molecular islands growing from chiral kink sites.[21] Flat adsorption configurations have been proposed for these structures. While the bonding of cysteine on Au has been investigated in terms of bonding configuration and changes in the density of states (DOS) for adsorption on the Au(111) surface,[26,27] this is not the case for the Au(110) surface. Especially the possible contribution of a bonding via the amino group and its interplay with the thiolate bond in the formation of a flat or perhaps a vertical adsorption geometry needs a deeper understanding. Complexity arises from the two bonds, possible charge transfer, interface dipoles, the influence of the bonding geometry, molecular deformation, and surface relaxation.

This work aims at elucidating the main mechanisms for the molecule adsorption. For this reason, in the present work the isolated S-Au and N-Au bonds of cysteine on Au(110) but also their interplay upon cysteine adsorption are studied by DFT total-energy calculations. Special emphasis is put on the analysis of the changes in the electronic structures of molecule and substrate during the adsorption, the filling of the electronic states as well as the accompanying electron transfers. The paper is structured as follows. In Sec. II we describe our computational methods. Sec. III contains the results for isolated bonds and in Sec. IV we present a complete picture of the cysteine adsorption. Finally, in Sec. V a brief summary and conclusions are given.

II. COMPUTATIONAL METHODS

The calculations are carried out in the framework of the DFT using a semilocal approximation for exchange and correlation in the generalized gradient approximation (GGA) as parametrized by Perdew and Wang.[28,29] Gradient corrections in the form of the PW91 functional have been shown to be superior to the local density approximation for the description of amino-acid bonds.[30] The pseudopotentials and wave functions are generated within the projector-augmented wave method.[31] The electron wave functions in the regions between the cores are expanded in a plane-wave-basis setup to a cutoff energy of 500 eV. This allows for an accurate treatment of the first-row elements as well as the Au $5d$ electrons.[30,32,33] The Brillouin zone integrations are represented by sums over Monkhorst-Pack points.[34] Energy con-

vergence with respect to these parameters was carefully checked. The ionic relaxations were performed until the Hellmann-Feynman forces acting on each ion were below 0.02 eV/Å. Specifically the *Vienna ab initio simulation package* (VASP) (Ref. 35) is applied. In order to model the adsorbed Au(110) surface we use the repeated slab method. Each supercell contains five Au layers (plus the adsorbed molecule) and a vacuum region equivalent in thickness to ten atomic layers. The lateral cell size was chosen as a 4×4 supercell. This methodology was found to yield converged surface energies of 91.5 meV Å^{-2}. Similar approaches reproduce the measured geometries for adenine adsorbed on Cu(110).[36] We mention that the used GGA functional[28,29] allows for a very reasonable description of covalent and metallic bonds with a tendency to slightly overestimate the bond lengths, e.g., yielding a gold lattice constant a_0=4.172 Å.[37]

Previous work on the missing-row reconstructed Au(110)-(1×2) surface, which is the most stable reconstructed clean surface, showed that cysteine adsorption removes the missing-row reconstruction,[19] thus creating an unreconstructed (1×1) surface, which we use here as substrate for cysteine adsorption. Our test calculations showed that the atoms forming the top rows of the missing-row reconstruction are likely to be removed in the presence of the adsorbate molecule, thus lifting the (1×2) reconstruction. Such a tendency has also been observed within another DFT study.[20]

III. ISOLATED ADSORBATE-SUBSTRATE BONDS

A. The thiolate-gold bond

1. Bonding geometry

To probe the interaction of the thiol head group -SH with the Au-(110)-(1×1) surface, we calculated the adsorption energies for various deprotonized configurations. The cysteine molecule was placed at sites on a regular mesh of points over the surface unit cell. For each adsorption site we optimized the height of the sulfur atom by a total-energy minimization. The orientation of the molecule was chosen to maximally restrict the interaction with the surface to the thiolate head group and kept fixed throughout all calculations. Comparison of the adsorption energies revealed the favored bonding positions of the thiolate head group to be bridge and off-bridge positions [cf. Fig. 1(b)]. At these positions S binds to two Au atoms. The bonding energy and, hence, the preferred adsorption site depends on the bond angles. The energy gain with respect to the nonbonded radical and clean surface varies strongly with the bonding geometry, ranging from 1.7 to 2.3 eV. Taking the optimized geometry into account, we obtain the $[1\bar{1}0]$ off-bridge position with the S atom about 1.6 Å above the Au surface layer to be the most favored site. The bonding geometry seems to favor a local tetrahedron geometry as also suggested by calculations of S-Cu bonds on a Cu(110) substrate.[38]

In order to quantify the dependence on the bonding angle, a series of calculations was carried out, in which the position of the S atom relative to the surface was kept fixed and the orientation of the rigid molecule was varied. For both bridge and off-bridge S adsorption sites the tilted geometries can be

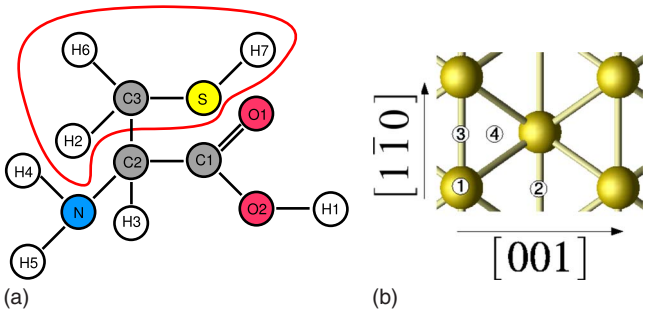

FIG. 1. (Color online) (a) Used notation for atoms of cysteine. The red enclosed area marks the side group that is replaced by –H for the glycine calculations (see text). (b) Unreconstructed (110) surface unit cell. High symmetry positions are indicated as follows: top site (1), [001] bridge site (2), $[1\bar{1}0]$ bridge site (3), and $[1\bar{1}0]$ off-bridge site (4).

described by just one angle α (cf. Fig. 2). The two nearest gold atoms serve as reference points and the angle is measured with respect to the mid position between these two atoms. We introduce two vectors for the definition of α. The vector $\boldsymbol{b}$ points from the sulfur atom to the mid position between the two Au atoms (bridge) and the vector $\boldsymbol{c}$ points from S to C3 [nomenclature is presented in Fig. 1(a)]. Both vectors have no component in $[1\bar{1}0]$ direction if S is located at $[1\bar{1}0]$ bridge or off-bridge site. The tilt angle is given by

$$\alpha = \arccos\left(\frac{\boldsymbol{b}\cdot\boldsymbol{c}}{|\boldsymbol{b}||\boldsymbol{c}|}\right). \tag{1}$$

In perfect tetrahedron geometry this angle would be $\alpha_{tetr}=\arccos(-1/\sqrt{3})\approx125.26°$. This geometry, however, would require an Au-S-Au angle of 109.5° and, hence, given an Au-Au distance of $a_0/\sqrt{2}$=2.95 Å between the two gold atoms, a S-Au bond length of 1.81 Å. This would be significantly smaller than the sum of the covalent radii 2.36 Å.[39] In fact, the calculated equilibrium bond length is 2.45 Å so such an ideal tetrahedron geometry is not possible. In contrast, the Au-S-Au angle amounts to 77.8°. Ideal tetrahedrons are obtained by an even division of the whole of angular space among four vectors, i.e., by maximizing the angle between all pairs of vectors (the result of which is 109.5°). Since in our distorted tetrahedron, two of the vectors are moved closer to each other, and the angle Au-S-Au is re-

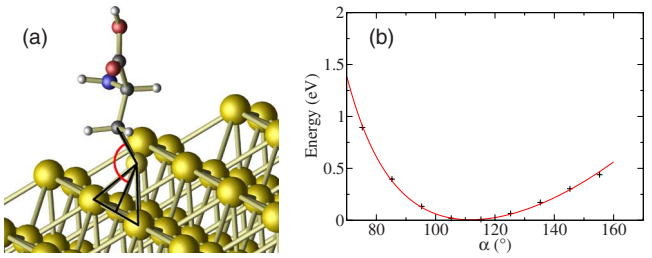

FIG. 2. (Color online) (a) Illustration of the tilt angle α (in red) between the Au bridge atoms and the S-C3 bond in the thiolate bonding configuration. (b) Energy variation versus the tilt angle α of the thiolate bond at the $[1\bar{1}0]$ off-bridge site.

duced to 77.8° the other angles can be larger and, consequently, α will be smaller than the optimal value of 125.26°. We therefore expect the optimal value for our bond angle α to be smaller than the ideal 125.26°.

Figure 2(b) shows the energy change in the system with varying α. The energy minimum is found at $\alpha_{opt}=111.8°$. As can be seen, the influence of the thiolate binding geometry on the system energy is considerable. Deviations of about 40° from α_{opt} give energy changes up to 0.8 eV. As expected, the optimal angle α_{opt} decreased from the ideal tetrahedron value 125.26°–111.8°. Since $0 \leq \alpha \leq 180°$, there are two possible conformations for a given value of α. However, if S is located at an off-bridge site, one of these two conformations would lead to the molecule being directed toward or even into the surface. Consequently, these conformations are not considered. This observation is in contrast to the common belief in literature that the optimization of the bonding geometry is not important for finding the lowest energy configuration.[40]

2. Electron transfer

The optimized S-Au bond length of about 2.45 Å is very close to the sum of the covalent radii 2.36 Å of sulfur (1.02 Å) and gold (1.34 Å).[39] Therefore, one might expect a strong covalent contribution to the thiolate bonding. Another indication for covalent bonding was found from the analysis of the optimal angle α and the resulting tetrahedron geometry. In order to gain deeper insight into the nature of the thiolate-gold bond we investigate the redistribution of the electron density. A molecule adsorbed at the [001] bridge site with $\alpha=\alpha_{opt}$ is used to study the bonding characteristics of the thiolate bond. The spatially resolved charge-density difference is computed according to

$$\Delta\rho(\boldsymbol{x}) = \rho_{ads/sub}(\boldsymbol{x}) - \rho_{ads}(\boldsymbol{x}) - \rho_{sub}(\boldsymbol{x}), \tag{2}$$

where $\rho_{ads/sub}$ is the charge density of the adsorbate-substrate system and ρ_{ads} and ρ_{sub} are the charge densities of the adsorbate without surface and the clean surface, respectively. Thereby, the isolated systems have the same geometry as in the combined structure. The charge-density difference is plotted in Fig. 3 and exhibits dominating contributions from sulfur-centered orbitals and the gold atoms involved in the bonding. In the molecule we observe charge redistribution in the regions of the sulfur sp^3 hybrids in tetrahedron geometry. There is electron depletion in the area corresponding to the Au d lobes and electron accumulation along the bond axis, which corresponds to a σ-type bonding orbital. The accumulation/depletion regions indicate that the thiolate-gold bond is due to localized interaction, i.e., electronic rearrangement occurs largely at the sulfur atoms and the contributing gold atoms. Symmetrical positions of S and C3 with respect to the surface structure give rise to largely symmetric charge redistribution patterns, which shows that the contribution of the asymmetrical tailgroup to the bond is small.

The complicated charge redistribution plotted in Fig. 3 shows positive and negative values, as discussed above, however, it does not allow for an estimate of the net transfer of charges between the gold substrate and the deprotonized cysteine radical. Such an electron transfer would be important for an electrostatic contribution to the binding energy. Moreover this is highly relevant for consideration of geometries with a simultaneous bond of the sulfur head group and the amino group to the surface. Electrostatic effects may also strongly influence the molecule-molecule interaction and lead to chiral recognition effects.[41]

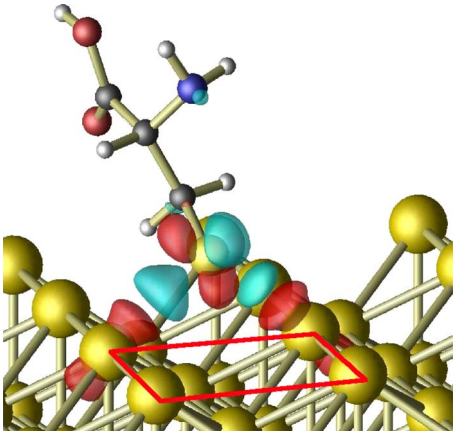

FIG. 3. (Color online) Charge-density-difference plots for the thiolate bond, S at [001] bridge site. Regions of electron accumulation/depletion are marked in blue(+)/red(−). Isosurface value: $\pm 0.025e$ Å^{-3}. The surface unit cell is indicated.

In order to analyze the charge transfer, in the first step we laterally integrate over $\Delta\rho(\boldsymbol{x})$, i.e., we calculate the total charge difference in a plane of thickness dz at given height z

$$\Delta Q(z,dz) = \int_{z}^{z+dz} d^3x \Delta\rho(\boldsymbol{x}) \tag{3}$$

and in a second step the total charge transfer into the Au(110) substrate

$$Q(z) = \int_{z_0}^{z} \Delta Q dz, \tag{4}$$

where z_0 is a position in the vacuum far from the surface. Charge difference $\Delta Q(z,dz)$ and total charge transfer $Q(z)$ are shown in Fig. 4. The adsorption results in electron accumulation ($\Delta Q>0$ and Q increasing) at the clean lower surface and a region of electron depletion ($\Delta Q<0$ and Q decreasing) at the upper surface to which the cysteine is attached. This charge distribution amounts to a net dipole moment in the gold slab, which is induced by the adsorbate. The overall dipole moment of the supercell containing adsorbate and substrate is calculated to $|\boldsymbol{p}_{ads/sub}|=2.74$ D in the direction of the surface normal. Most of this dipole moment, however, is not due to adsorption-induced electron rearrangement. It is caused by the deprotonization of the cysteine radical, as can be seen by investigating the polarization of the supercell containing only the free cysteine radical. Here, the calculated dipole moment is $|\boldsymbol{p}_{ads}|=2.37$ D. Figure 4 shows considerable charge transfer within the molecule with aggregation regions at the upper atoms and electron reduction in the central areas of the adsorbed radical. Consequently multipole moments of higher order are likely to play a role in this bond. Besides the above-mentioned polarization

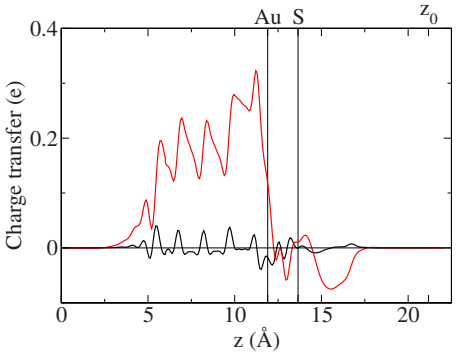

FIG. 4. (Color online) Total-charge difference for the thiolate bond, S at [001] bridge site: total-charge difference $\Delta Q(z)$ at given height z (black) and total-charge transfer from above z to below $Q(z)$ (red). The position of the Au top layer, the position of S, and z_0, the starting point of the integral in Eq. (4), are marked.

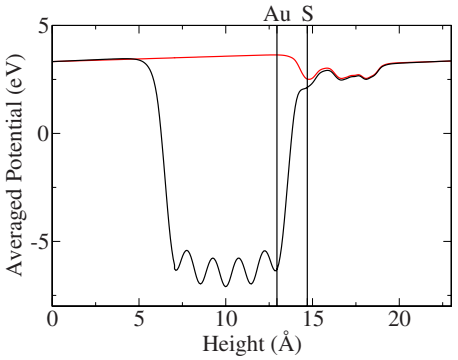

FIG. 5. (Color online) Plane-averaged potential of adsorbate-substrate system (black) and free deprotonized cysteine radical (red). The position of the top-row Au layer and the S atom are indicated. The vacuum levels (plateaus) outside the systems are aligned.

of the gold slab we do not observe a net charge transfer from the molecule to the surface (Q oscillating around zero between Au and S), ruling out the possibility of an ionic contribution to the binding energy.

3. Electronic-state changes

The adsorbate bonding due to S-Au interaction and the accompanying electron redistribution have consequences for the electronic structure in the adsorbate system with respect to the gas-phase amino-acid molecule and the clean metal surface. We investigate these changes in terms of the Kohn-Sham (KS) eigenvalues of DFT and the corresponding DOS of the adsorbate system, the free molecule and the metal surface. In doing so, we should keep two points in mind. First, the KS eigenvalues do not account for the excitation aspect and quasiparticle character of single-particle electronic excitations.[42] However, these effects mainly influence the energetical distance of occupied and unoccupied states,[30] and occur in the adsorbed as well as the gas-phase molecule. For the metal, these effects vanish close to the Fermi level.[42] Second, comparing the DOS of two different systems—adsorbate and molecule—one has to deal with three different energy scales which are significantly influenced by the local electrostatics. We solve this problem by aligning the energy scales by means of the electrostatic potentials from the KS equation. More precisely, we use plane-averaged potentials where the planes are parallel to the surface. The vacuum level in the potentials of the three systems are used for the energy-scale alignment (see Fig. 5). There are however two problems associated with the vacuum-level-alignment method. The first is that due to surface dipoles and electron density tailing the vacuum level close to interfaces or molecules is not equal to the vacuum level in larger distances.[2] Since we are using the vacuum level right above the cysteine radical for the alignment, this problem does not apply to our system. The second is that both our systems possess an overall dipole moment that—due to the periodic boundary conditions of the DFT supercell approach—adds a sawtooth shape to the electrostatic potential. But since the dipole moment is almost the same for both adsorbate system and free radical, a reasonably good alignment can nevertheless be obtained.

Results for the total DOS and its projection onto several sets of atoms, i.e., the projected DOS (PDOS), are shown in Fig. 6. We project to the metal substrate and the molecule separately by summing up over the corresponding metal slab and molecule atoms. In comparison, the DOS of the free cysteine radical is also plotted. A refined analysis takes care of the character of the wave function by projecting onto the s, p, and d states of the considered atom as well. The band extending from about 2–6 eV below the Fermi level in Fig. 6(a) is characteristic for the Au d orbitals. The Au PDOS is only marginally affected by the single-molecule adsorption. Significant changes, however, occur for the adsorbate [cf. Fig. 6(b)]. The most noticeable difference between molecule-projected density of states in the gas phase and the adsorbed state is the disappearance of the sharp, distinct highest occupied molecular orbital (HOMO) peak at −0.8 eV of the gas-phase radical upon adsorption. The HOMO of the free deprotonized cysteine radical is localized at the sulfur atom as evident from Fig. 6(c). Therefore, the most pronounced changes are observed in the DOS projected on the S atom.

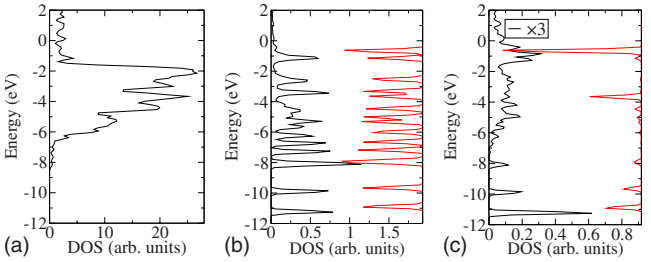

FIG. 6. (Color online) (a) Au PDOS of the adsorbate-substrate system. (b) Cysteine-radical PDOS of the adsorbate-substrate system (black) and of the free cysteine radical (red, from right to left). (c) S PDOS of the adsorbate-substrate system (black) and of the free cysteine radical (red, from right to left). The S PDOS of the adsorbate-substrate system has been magnified by a factor of 3 to allow for better visibility of the lineshape. Energy alignment was obtained using the vacuum level of the electrostatic potential. The energy zero is set to the Fermi level of the metal.

The S-projected DOS shows considerable broadening for all S-localized states above −7 eV. In particular, we find a rather broad distribution over the energy interval between 0 and −6 eV, which is the range of the Au *d* orbitals. There are small peaks at the upper and at the lower end of this distribution, indicating a hybridization into bonding and antibonding states. Sulfur PDOS peaks below the main region of the Au *d* bands and all other molecular orbitals are unaltered in shape and slightly shifted to lower energies. The weak modifications in molecular states which are either not localized on sulfur or which, if localized on sulfur, are not in the energy range of the Au *d* states lead to the following final conclusions: (i) the molecule-substrate bond is strongly localized at the sulfur atom. (ii) Rehybridization of orbitals leads to a bond with sp^3 character. (iii) Electrostatic effects do not play a significant role.

B. The amino-gold bond

1. Geometry and energetics

In order to probe the bonding properties of cysteine via the NH_2 amino group on the Au(110) surface, a series of calculations analogous to the calculations describing the thiolate-gold bond is carried out, in which the molecule is placed at different locations on a three-dimensional mesh and the corresponding adsorption energies are determined. To investigate the Au-amino bond in isolation, it is important to restrict the molecule-gold interaction to the amino-group nitrogen. Such a study of an isolated amino bond to a metal is possible for a flat moleculelike adenine[9,43] or ammonia,[10] where no additional sidegroups give rise to bonding contributions interfering with the Au-amino bond. In the case of cysteine, however, this is not possible due to steric effects. In order to avoid additional interactions besides the amino-group Au bond which may be caused by the remaining parts of the molecule, we reduce the molecule by replacing CH_2-SH [see Fig. 1(a)] by H which gives the closely related amino-acid glycine. The resulting structure closely resembles the most stable glycine conformation with the amino group pointing away from the C1-C2 axis at almost a tetrahedron angle.[32]

From a series of total-energy calculations on a regular mesh of possible molecule positions we obtain a minimum position very close to the top site [cf. Fig. 1]. In this off-top position the height of the amino-group nitrogen is 2.2 Å above the topmost Au layer. The energy gain due to bonding with respect to the free molecule and surface amounts to 0.53 eV. This is significantly larger than for amino-group bonding on Cu(110).[43] Similar to the findings of Ref. 43, although maybe not so pronounced, the energy can be assumed to be a lower limit due to the incorrect description of the van der Waals interaction (see also Refs. 6 and 44).

2. Electron transfer

The interpretation of the amino-Au bond is difficult. On the one hand, the amino group and the N-C bond remain intact. On the other hand, the N-Au distance of 2.26 Å approaches the sum of the covalent radii of Au (1.35 Å) and N (0.75 Å),[39] indicating a strong bond. For a better understanding we again calculate $\Delta\rho$ according to Eq. (2).

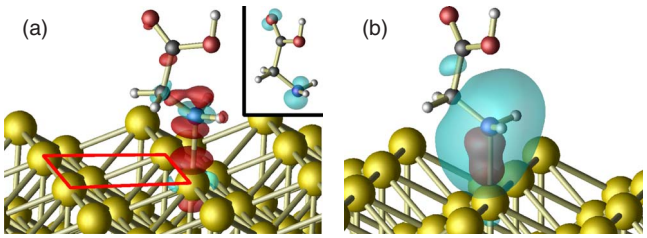

FIG. 7. (Color online) (a) Charge-density difference for the amino bond, N at top site. Regions of electron accumulation/depletion are indicated in blue(+)/red(−). Isosurface value: $\pm 0.025e$ Å^{-3}. The surface unit cell is indicated. The inlet depicts the free glycine HOMO, isosurface value: $0.3e$ Å^{-3}. (b) Isosurfaces of the spatially resolved electrostatic potential difference $\Delta V_{el}(\boldsymbol{x})$ (5). Isosurface values are −1 (blue) and −2 (red) eV.

Figure 7(a) shows isosurfaces of $\Delta\rho$ for N at top site, i.e., slightly displaced from the most favorable site. The size of the isosurface-enclosed regions indicates the amount of charge transfer. The redistribution of the electrons is concentrated around the amino nitrogen and the nearest gold atom. The regions of electron depletion above and below the interacting Au atom show the characteristic shape of *d* electron orbitals which were already observed in the charge redistribution due to the Au thiolate bond. Smaller contributions are found in the region of the N-C2 bond. Charge redistributions in the molecule are best represented by the glycine HOMO, which is also depicted in Fig. 7(a). It is predominantly located at the amino-group nitrogen and coincides with the region of electron depletion. So far, the emerging picture of the bond consists of electron rearrangement due to interaction of the HOMO state with the Au *d* orbitals. In this regard, the bonding of the amino group seems to be rather similar to the bonding of the sulfur head group discussed in Sec. III A. In the following however, we discuss why it is not. A closer look at the Au-N bond axis and the Au-S bond axis in Figs. 7 and 3, respectively, reveals the signs along the axis (red/blue) being different. While the Au-S bond exhibits a change in sign along the bond axis, this is not the case for the amino-gold bond, where only red lobes are visible along the Au-N axis. The complexity of the depletion and accumulation regions in Fig. 7(a) does not indicate covalent or ionic bonding but the above findings might have an influence on the total-charge transfer.

In order to determine the total-charge transfer from adsorbate to substrate we calculate $\Delta Q(z)$ and $Q(z)$ according to Eqs. (3) and (4). The results of this procedure are plotted in Fig. 8. We observe charge accumulation at the lower and, especially, at the upper surface of the slab. Inside the slab the charge rearrangements are periodical alternations of accumulation and depletion that cancel each other out. As can be seen, the total-charge transfer depends strongly on where we draw the dividing plane z_d between slab and molecule. However, since the maximum total-charge transfer lies approximately halfway between the topmost Au layer and the amino-nitrogen atom, it seems appropriate to place z_d at the height of maximum charge transfer. The total-charge transfer

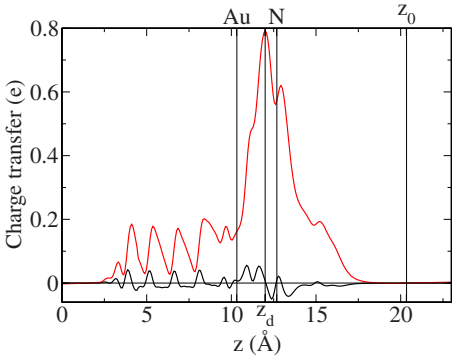

FIG. 8. (Color online) Total-charge difference for the amino bond, N at top site: total-charge difference $\Delta Q(z)$ at given height z (black) and total charge transfer from above z to below $Q(z)$ (red). The position of the Au top layer, the position of N, the starting point of the integral z_0 from Eq. (4) and the dividing plane z_d are marked.

from molecule to surface $Q(z_d)$ is 0.79 electrons for N at top site. The picture that presents itself here is that electrons are transferred from the adsorbate into the substrate. The excess charge in the slab, however, is not spread out through the whole gold slab but transferred to its surfaces. The nonvanishing charge transfer indicates an electrostatic contribution to the bond and should have visible consequences on the electronic structure of the adsorbed molecule.

Such an electrostatic effect can be visualized by computing the spatially resolved adsorption-induced potential difference

$$\Delta V_{el}(\boldsymbol{x}) = V_{el}^{ads/sub}(\boldsymbol{x}) - V_{el}^{ads}(\boldsymbol{x}) - V_{el}^{sub}(\boldsymbol{x}). \tag{5}$$

This quantity is presented in Fig. 7(b). There is a region of considerable potential shift centered at the N-Au bond axis and reaching up to the molecule.

The above findings are not particular to the chosen adsorption site. $\Delta\rho$, $\Delta Q(z)$, and $Q(z)$ were determined and investigated for other bonding sites as well. The charge-density-difference isosurfaces showed patterns very similar to those displayed in Fig. 7(a) but the enclosed regions are smaller for other adsorption sites. We find that the configuration with the largest charge transfer coincides with the strongest molecule-substrate bond, which supports the description of the bond between amino group and transition metal in terms of Coulomb interaction, as proposed previously for adenine on Cu(110).[43]

3. Electronic state changes

The above-described charge redistribution of nearly one electron upon adsorption with N at top site implies considerable changes in the electronic DOS. This is analyzed by means of the site-projected density of states for free and adsorbed molecule as well as the Au slab, shown in Fig. 9. In the gas phase the glycine HOMO peak appears at −1 eV [see Fig. 9(b)]. This peak is not present in the glycine-projected DOS of the adsorbed system. The projection onto the amino-group nitrogen [Fig. 9(c)] reveals that the glycine HOMO is mainly localized at N in the gas phase. The interaction with the surface, however, either depopulates this orbital or shifts it to another energy, possibly accompanied by a broadening. In view of the findings from the charge-transfer analysis, which revealed a considerable electron depletion at the molecule, all molecular states should undergo such a shift. Indeed, Fig. 9(b) shows that the HOMO-10 (at −11 eV) is shifted by −1 eV upon adsorption. Similarly, higher-energy states experience also a downward shift which is consistent with a loss of electrons in the molecule. The potential difference depicted in Fig. 7(b) gives rise to the downwards shift in energy for all amino-group-localized states as observed in Fig. 9(b). The new HOMO state is considerably broadened and slightly decreased in energy. The picture we get of the Au-amino bond is, that through interaction with the Au *d* orbitals the glycine HOMO state is rearranged and charge is transferred from the area of the amino group into the slab, thus causing considerable amino-localized potential shifts and introducing multipole moments in both adsorbate and substrate. The monopole attraction, visible in the adsorption-induced shift of molecule-localized states to smaller energies, causes considerable attraction moderated by multipole interactions. The symmetry and localization of the electron redistribution depicted in Fig. 7(a) as well as the conservation of the lineshape of the glycine-projected DOS not localized at the amino group as discussed above implies that the contribution of the molecular tail to the Au-amino bond is small. Therefore our findings regarding the adsorption of glycine should hold for cysteine adsorption as well. However, whether the single-bond properties discussed in this section still hold upon simultaneous bonding via the amino-group nitrogen and the thiolate-group sulfur remains to be seen.

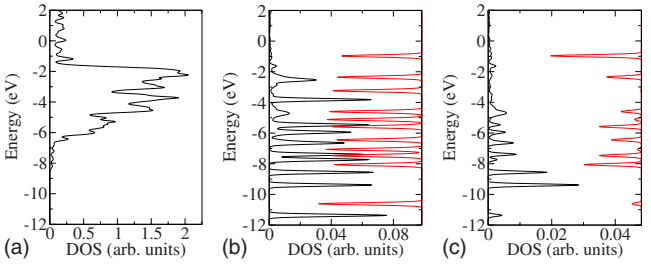

FIG. 9. (Color online) (a) Au-projected DOS of the adsorbate-substrate system. (b) Glycine-projected DOS of the adsorbate-substrate system (black) and of the free glycine molecule (red, from right to left). (c) N-projected DOS of adsorbed (black) and gas-phase (red, from right to left) system. The Fermi level of the metal is used as energy zero.

IV. MOLECULE ADSORPTION

A. Relaxed geometries

The two possibilities for the bonding of a cysteine molecule (via the amino- and the thiol-side groups) and the accompanying energy gains suggest an adsorbate geometry with two bonds, if the cysteine molecule can still register to the Au(110) surface and its deformation does not cost too much elastic energy. When one takes into account the parameters influencing the adsorption energy of the cysteine radi-

TABLE I. Bond angles in degrees of relaxed adsorbed and gas-phase cysteine configurations.

Configuration	1	2	3	Upright	Gas phase
α	120.0	117.7	127.7	119.2	
Au1-S-C3	113.8	111.8	115.6	107.3	
Au2-S-C3	109.7	104.0	111.5	114.7	
Au1-S-Au2	84.1	97.3	98.6	85.6	
S-C3-C2	117.4	114.8	119.8	108.8	113.4
C3-C2-C1	109.4	108.6	109.9	110.1	109.9
C3-C2-N	114.4	111.9	113.6	110.8	110.7
Au-N-C2	118.5	124.8	118.2		
C2-N-H2	109.8	109.9	110.8	111.0	110.3
C2-N-H3	111.3	110.4	109.9	111.4	110.8
H2-N-H3	109.1	106.0	107.8	107.5	106.9

cal, i.e., position of S and NH_2, the thiolate bonding angle and the intramolecular strain, flat adsorption geometries seem to be energetically favored over upright configurations.

In order to prove this hypothesis we have studied three qualitatively different flat adsorption geometries—registering to the surface via both the amino-side group and the thiolate head group and one upright configuration—registering solely via the thiolate group and compared the corresponding results. The resulting geometries can be seen in Fig. 11. The three flat adsorbate configurations differ with respect to the positions of the amino and thiolate bonds. Configuration 1 has N at an off-top site and S at the $[1\bar{1}0]$ bridge site.[45] Configurations 2 and 3 both have N at a top site and S at the [001] bridge site but differ from each other due to the chirality of the molecule. The upright configuration has S at the most favored $[1\bar{1}0]$ off-bridge site.

The bond angles and bond lengths are listed and compared with parameters of the gas-phase cysteine molecule in Tables I and II. Hereby, we use conformer 9 of Ref. 30, the geometry of which is closest to the geometry of the adsorbed molecule. The tables demonstrate that the bond lengths are almost conserved and are essentially the same in different adsorbate configurations. More important are the variations in the bond angles in the adsorbate-substrate bond region. A comparison of the bond angles in Table I shows that the thiolate bond angles Au-S-C3 are close to the tetrahedron angle 109.4° in all four configurations (see discussion in Sec. III A 1). The Au1-S-Au2 angles, however, are considerably smaller due to the S-Au and Au-Au bond lengths, which are incommensurable with an ideal tetrahedron geometry. This holds especially for configuration 1 and the upright configuration since both have S located at the short $[1\bar{1}0]$ bridge site. In the case of configuration 1 and the upright configuration, the value of α seems puzzling at first glance since it is significantly different from the optimal value of 111.2° determined for exactly that position in Sec. III A 1. This however is due to adsorption-induced surface rearrangements (see Sec. IV C). While the adsorption configurations with S located at the [001] bridge site causes the Au atoms engaged in the thiolate bond to be lifted above the rest of the surface and toward S, adsorption with the sulfur head group near the $[1\bar{1}0]$ bridge (configuration 1 and upright) causes the Au atoms to be elevated too, but laterally relocated away from S, thus widening the Au-S-Au angle. This displacement is due to the preferred tetrahedron structure of the thiolate bond, and, as has been discussed in Sec. III A 1, increases α, bringing it closer to the tetrahedron value of 125.26°. The intramolecular bonding angles remain close to their gas-phase values, only S-C3-C2 varies significantly.

We have to mention that configuration 3 possesses one extra molecule-substrate bond. In addition to the interaction with the amino and thiolate group, there is a hydrogen bond between H3 and the metal slab. Table II shows an increase in the C2-H3 bond length by 0.02 Å.[46] If we use the lengthening of the carbon-hydrogen bond as an indicator for the bond strength, we can estimate the bond to have an energy of 0.2 eV or more. We estimate the amino bond of configuration 3 to be noticeably weaker then in configuration 2. The additional bond is probably the reason that configuration 3 is nevertheless energetically slightly more favorable.

Comparing our adsorption configurations with those of earlier experimental and theoretical studies[19,20] of cysteine adsorption on Au(110), we see our findings regarding the most favorable adsorption geometry in agreement with these works. Although the geometries proposed by Kühnle *et al.* are dimer adsorption geometries they too exhibit the preference of the thiolate group to bind at the $[1\bar{1}0]$ off-bridge site that causes the amino group to move from its favored top position to an off-top position.

TABLE II. Bond lengths in Å of relaxed adsorbed and gas-phase cysteine configurations.

Configuration	1	2	3	Upright	Gas phase
Au1-S	2.43	2.46	2.47	2.41	
Au2-S	2.43	2.48	2.47	2.42	
S-C3	1.84	1.84	1.84	1.84	1.82
Au-N	2.36	2.35	2.33		
N-C2	1.48	1.48	1.48	1.46	1.46
Au-H3			2.38		
C2-H3	1.10	1.10	1.12	1.10	1.10

B. Adsorption energies

Since the bonding of cysteine to the Au substrate is accompanied by a dissociation of the molecule into a cysteine radical and a hydrogen atom, the computation of the binding and adsorption energies requires the knowledge of the hydrogen chemical potential. We assume that the hydrogen atoms dissociated from the cysteine form molecules. For that reason we consider the total energy E_{H_2} of the gas-phase H_2 molecule. The total-energy optimization for the H_2 molecule with respect to the bond length was performed, using a cubic supercell of 10 Å edge length in the DFT framework described in Sec. II. Energy convergence with respect to cell size has been carefully checked. The system was relaxed until the residual forces were below 0.01 eV/Å for each

TABLE III. Adsorption energies with respect to the free deprotonized cysteine radical ΔE_{rad}^{ads} with respect to the gas-phase cysteine molecule ΔE_{mol}^{ads} and slab deformation energy ΔE_{sub} of cysteine Au(110) adsorbate configurations in eV. Displacements of top-layer Au atoms in Å. Au1 and Au2 are the atoms binding to S, Au3 the atom binding to N. Positive values describe displacement toward the bonding partner, negative values away from the bonding partner. x, y, and z stand for the [001], the [1$\bar{1}$0], and the [110] direction, respectively.

Configuration	ΔE_{rad}^{ads}	ΔE_{mol}^{ads}	ΔE_{sub}	Atom	Δx	Δy	Δz	$\lvert\Delta \boldsymbol{x}\rvert$
1	−2.637	−0.743	0.270	Au1	−0.06	−0.17	0.19	0.26
				Au2	−0.10	−0.14	0.19	0.26
				Au3	0.01	0.04	0.09	0.10
2	−2.501	−0.607	0.246	Au1	0.24	0.06	0.12	0.28
				Au2	0.22	0.04	0.13	0.26
				Au3	0.07	0.10	0.06	0.14
3	−2.526	−0.632	0.254	Au1	0.22	0.04	0.13	0.26
				Au2	0.21	−0.06	0.16	0.27
				Au3	0.07	0.05	0.04	0.09
upright	−2.166	−0.272	0.292	Au1	−0.05	−0.20	0.16	0.26
				Au2	−0.11	−0.13	0.28	0.32

proton. The resulting molecular bond length of 0.75 Å is in good agreement with its literature value [0.74 Å (Ref. 47)].

Besides E_{H_2}, we need the total energies $E_{ads/sub}$ of the slab with adsorbate, E_{sub} of the clean substrate, E_{rad} of the deprotonized gas-phase cysteine radical, and E_{mol} of the intact gas-phase cysteine molecule to compute the characteristic energy gains. The adsorption energies with respect to radical and molecule are then calculated as

$$\Delta E_{rad}^{ads} = E_{ads/sub} - E_{sub} - E_{rad} \tag{6}$$

and

$$\Delta E_{mol}^{ads} = E_{ads/sub} + \frac{1}{2}E_{H_2} - E_{sub} - E_{mol}. \tag{7}$$

The computed energies are listed in Table III. Configuration 1 is the energetically most-favored adsorption configuration while configurations 2 and 3 are energetically very close to each other but 0.1 eV higher than configuration 1. The energy gain due to an upright adsorbate geometry is much smaller. We conclude that the docking of the cysteine via both the amino N atom and the thiol S atom gives rise to flat adsorption geometries as the most favorable ones.

Comparing the three considered flat adsorption geometries, we find that the binding energy depends on the registering of the adsorbate molecule at the surface. The docking at off-top site (N) and [1$\bar{1}$0] bridge site (S), i.e., configuration 1, is finally favored. All four considered adsorption configurations are discussed below.

C. Adsorption-induced surface rearrangements

The investigation of spatial rearrangement of Au atoms gives us additional insight into the molecule-substrate interaction. All adsorption configurations with S at [001] bridge site cause the Au atoms engaged in the thiolate bond to be slightly lifted and laterally moved toward S while adsorption of the upright molecule and of configuration 1, which both have S localized at a [1$\bar{1}$0] off bridge site, shifts the Au atoms laterally away from the thiol group. The adsorption-induced displacement of all Au atoms engaged in bonds with the molecule was calculated as

$$\Delta \boldsymbol{x}_n = \boldsymbol{x}_{ads/sub,n} - \boldsymbol{x}_{0,n}, \tag{8}$$

where $\boldsymbol{x}_{ads/sub,n}$ and $\boldsymbol{x}_{0,n}$ denote the position of the ion n in the adsorbate/substrate system and in the clean relaxed slab, respectively. Table III contains the $\Delta \boldsymbol{x}_n$ for all atoms engaged in thiolate and amino bonds. The rearrangement is described for all three directions, where x, y, and z denote as usual the [001], [1$\bar{1}$0], and [110] direction, respectively. Positive values indicate displacement toward the bonding partner while negative values denote displacement away from the bonding partner.

One common feature of all atoms participating in thiolate bonds is that the lateral displacement exceeds the vertical shift. In configurations 2 and 3, the atoms are laterally repositioned toward S. For the configurations where the thiol group is placed near the short [1$\bar{1}$0] bridge, i.e., configuration 1 and the upright configuration, the displacement points laterally away from the thiolate group, thus effecting a thiolate binding geometry closer to tetrahedron structure. This relaxation away from the bonding partner underlines the important role that the bonding geometry plays in the Au-thiolate bond. As discussed in Sec. III A 1 the resulting widening of the Au-S-Au angle leads to an increase in the optimal bond angle α [Eq. (1)]. This explains the fact that α is found to be significantly larger than 111.8° in the relaxed geometries of configuration 1 and the upright configuration (see Table I). The repositioning of the Au atoms interacting with the amino group is considerably smaller than that of the thiolate bonding partners, as could be expected from the relative strengths of the bonds. It is most pronounced in configu-

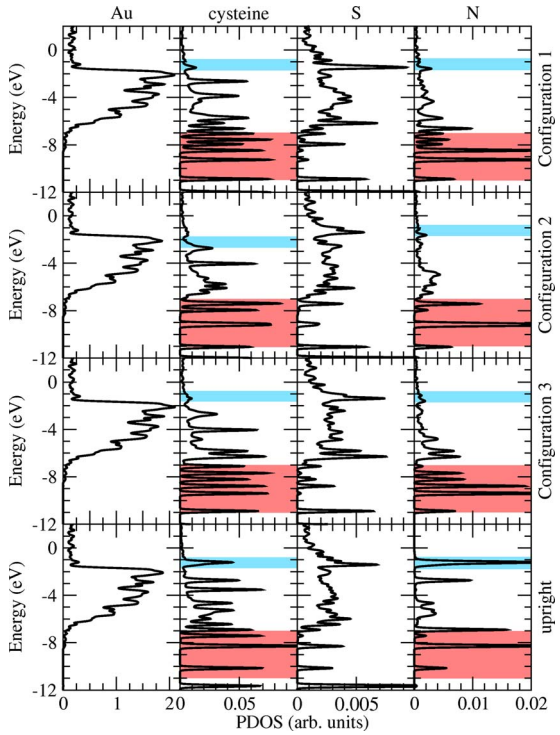

FIG. 10. (Color online) Au-projected, cysteine-projected, S-projected, and N-projected density of states of the four relaxed adsorbed cysteine configurations. The Fermi level is aligned with the origin of the energy scale. For colors, see text.

ration 2. Since the spatial displacement is a good measure for the "pull" exerted by the bonding partner, it seems that the Au-amino bond is strongest for this configuration.

The deformation energy due to adsorption-induced substrate rearrangement was calculated as

$$\Delta E_{sub} = E_{sub} - E_{sub,0}, \tag{9}$$

where E_{sub} and $E_{sub,0}$ denote the total energies obtained from calculations using the adsorption-restructured Au(110) slab and the clean relaxed slab, respectively. The results are listed in Table III. It is interesting that for the molecule adsorbed at the short bridge, i.e., for configuration 1 and the upright configuration, the strain is noticeably greater than for the adsorption geometries with the thiol head group at the long [001] bridge, indicating stronger bonds at the bridge site. The energy cost for the slab rearrangement for configuration 1 is about 20 meV greater than for the other flat adsorption geometries. Nevertheless, this configuration is energetically favored with respect to the other flat geometries by about 100 meV. This underlines the important role of the thiol-group docking site in the adsorption process.

D. Electronic-state changes

The flat adsorption geometries with their two docking bonds S-Au and N-Au give rise to redistribution of electronic states. This is demonstrated in Fig. 10 by means of the subsystem- and site-projected densities of states. The DOS-projected onto the Au(110) substrate states in Fig. 10 does seemingly not vary with the adsorption geometry studied, neither in the energy range of the Au *d* bands nor in the Au *s* region. In contrast, the effect of the adsorption configuration on the cysteine-projected DOS is much more significant. In order to understand the changes in more detail, the densities of states projected onto S and N, i.e., the atoms most influenced by the bonding, are presented too. One observes, that the differences in the cysteine-projected DOS of the four configurations are mainly due to differences in the amino-gold interaction. While the S-projected DOS has very similar shapes for all four configurations, the N-projected DOS displays the same differences as the molecule-projected DOS. Particularly the peaks below −6 eV, i.e., below the Au *d* bands possess the same lineshape as the cysteine-localized states (red shading). This indicates that the main difference in the adsorption characteristics of the configurations lies in variations in their Au-amino bond. This fact leads to an important conclusion. The final adsorption geometries are dominated by the stronger thiolate bond while the amino bond is largely formed within the constraints imposed by the intramolecular and preferred thiolate-bonding geometries.

In all flat adsorption geometries the amino-localized HOMO-1 state of the free molecule, equivalent to the glycine HOMO state discussed in Sec. III B 3, is largely suppressed and new peaks appear below the Au bands (blue shading). This confirms that in the amino-bonded system N-localized states are shifted downwards in energy due to N-localized regions of electron depletion, as discussed for the isolated bond in Sec. III B 3. The retaining of the N-localized HOMO-1 state in the upright molecule is a result of missing amino-Au interaction. The N-projected DOS of the upright molecule retains its gas-phase profile [compare with Fig. 9(c)] except a broadening of the states about 5 eV below the Fermi level probably due to intramolecular charge redistribution.

In all configurations the S-projected DOS shows the same pattern of bonding and antibonding states with peaks right above and below the Au *d* bands and a plateau between 2 and 5 eV below the Au Fermi level. This is the same basic pattern as observed in the case of the isolated thiolate bond [see Fig. 6(c)]. As discussed in Sec. III A 3, this lineshape is due to a hybridization of the S *p* orbitals with metal states forming bonding and antibonding states. A similar lineshape has also been found for thiolate-Au bonds on the Au(111) surface.[27] The fact that the nearby amino bonds do not alter qualitatively the lineshape of the thiolate-localized states supports our description of the S-Au bond as a localized interaction. The fact that the S-projected DOS remains qualitatively unchanged while the N-projected DOS varies in all relaxed configurations confirms the leading role of the thiolate bond in the adsorption process. We want to mention that the additional hydrogen bond in configuration 3 also changes the electronic states of the interacting hydrogen atom in the energy range of the Au *d* bands, indicating interaction with the *d* orbitals.

E. Electron transfer

The charge-density difference $\Delta\rho(\boldsymbol{x})$ is calculated according to Eq. (2) for all four configurations under discussion. In

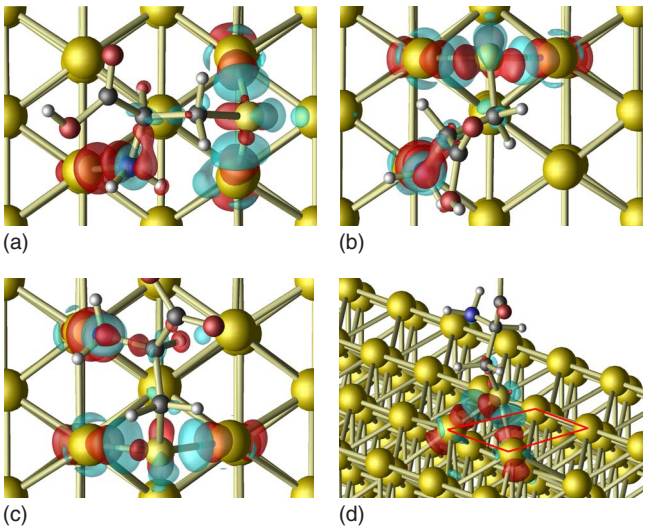

FIG. 11. (Color online) Charge-density difference plots for the relaxed adsorbed cysteine configurations. Regions of electron accumulation/depletion are marked of in blue(+)/red(−). Isosurface value: $\pm 0.025e$ Å^{-3}. (a) Configuration 1, (b) configuration 2, (c) configuration 3, and (d) upright configuration. In (d) the surface unit cell is indicated.

the calculation of $\Delta\rho(\boldsymbol{x})$ the isolated systems are taken at the geometry of the respective relaxed adsorbate-substrate systems. Figure 11 shows $\Delta\rho$ isosurface plots for the four configurations.

Qualitatively, the charge-density difference in all four systems resembles the differences caused by the isolated bonds, which indicates very similar bond characteristics. The amino-bond charge redistributions of configurations 1, 2, and 3 closely resemble the isolated amino-Au bond shown in Fig. 7. Note that in configuration 1 the red clouds denoting regions of decreasing electron density between N and Au are tilted due to the off-top location of N which renders them easily visible in a top view [left part of Fig. 11(a)]. In configuration 2 and 3 the accumulation regions centered at that Au atom have lost the symmetry of the isolated Au-amino bond due to asymmetrical charge redistribution and atomic displacements in the slab caused by the nearby thiolate bond. Configuration 1 displays far less electron accumulation at the Au atom interacting with the cysteine amino group. This indicates a weaker N-Au interaction and hence a weaker amino-Au bond than in the other two flat adsorption geometries, caused by the more disadvantageous off-top position. The largest isosurface enclosed regions at the site of the N-Au bond are observed in configuration 2. In this configuration, the patterns also have the closest resemblance to those of the isolated bond. This seems to indicate that in this geometry the Au-amino bond is stronger than in the other configurations.

For configurations 1 and 3, $\Delta\rho$ shows S-localized charge transfer patterns similar to the isolated thiolate bond (Fig. 3). Electron accumulation along the S-Au bond axes is asymmetrical and there is a region of decreasing electron density opposite the bond axis around which less charge accumulates. In configuration 2, the thiolate-localized charge redistribution displays nearly complete symmetry in [001] direction although the S-C3 bond does not lie in the (001) plane and the S-Au bond lengths are not entirely equal. The upright configuration shows a thiolate bonding pattern, that, although not entirely symmetric, displays more $[1\bar{1}0]$ line symmetry then both the model isolated thiolate bond and configurations 1 and 3, despite the fact that the S-C3 bond is considerably tilted with respect to [001]. Nevertheless the asymmetrical features of configuration 3 and of the isolated [001] bridge bond are visible, although less pronounced.

Configuration 3 shows one additional feature not present in the other configurations. The H3 localized electronic density decreases through adsorption and on the axis toward the upper right Au-atom there is a small area of electron accumulation [upper right side of Fig. 3(c)]. This pattern is due to the weak hydrogen bond mentioned above.

In our investigations of the isolated amino-Au bond [Sec. III B] we found that the charge transfer from molecule to substrate was largest for the adsorption site with the strongest bond. Therefore, the total-charge transfer can be used as an approximate measure for the strength of the amino bond. The total-charge transfers $Q(z_d)$ between amino-acid molecule and Au(110) substrate has been calculated for all four adsorption geometries according to Eq. (4). Equally to the procedure in Sec. III B 2, the dividing plane z_d was chosen at the position of maximum charge transfer for the flat adsorbed configurations (cf. Fig. 8). While for the upright configuration no net charge transfer was observed, we measure 0.51, 0.66, and 0.66 electrons for the configurations 1, 2, and 3, respectively, i.e., more than half of an electron is transferred from the molecule into the substrate. This is similar though somewhat less than in the case of the isolated bond discussed in Sec. III B (0.79 electrons). The largest total charge transfer is observed in configuration 2 (slightly larger than in configuration 3), which supports the assumption made above that the N-Au bond is strongest in this geometry.

The upright adsorption configuration shows a charge-transfer pattern similar to that of the isolated thiolate bond. We observe the characteristic polarization of substrate and molecule, and no net charge transfer from molecule to substrate. In the area between thiol head group and surface, however, there is considerably more charge redistribution than in the case of the isolated bond, an indication for stronger bonds. Since the isolated thiolate bond was investigated at the [001] bridge site with near-optimum geometry, it seems that the favored bonding site for the thiolate bond really is the $[1\bar{1}0]$ off-bridge site if a tetrahedronlike bonding geometry can be retained. This conclusion is also supported by the fact that the flat adsorption geometry with S located at the $[1\bar{1}0]$ bridge site is energetically most favored, although the low charge transfer indicates a weaker amino-Au interaction than in the other flat geometries.

V. SUMMARY AND CONCLUSIONS

We have studied the adsorption of the amino-acid-molecule cysteine on the relaxed Au(110)-(1×1) surface in detail by means of density-functional-theory calculations within the framework of a semilocal exchange-correlation

description and the projector-augmented wave method. The total-energy optimizations with respect to the atomic positions have been accompanied by investigations of the electron transfers and the changes in the electronic structure of both molecule and substrate upon adsorption. The studies were exclusively focused on the adsorption of single molecules (not of pairs, chains, or layers) and, in particular, on the possible adsorbate geometries—flat versus upright configurations. To understand the driving forces for the adsorption and the formation of adsorbate geometries we have investigated the possible docking of the cysteine via only one of its sidegroups.

For the isolated thiolate-Au bond, fragmentation of the molecule in a radical and a hydrogen atom is important. The $[1\bar{1}0]$ off-bridge and the [001] bridge adsorption sites were found to be the energetically most favorable positions of the thiolate head group. We observed localized electronic interaction and hybridization of S-derived states in the S-projected density of states of the thiolate-bonded system. These are similarities with findings for the Au(111) surface. The binding energy was demonstrated to be strongly determined by the bonding geometry. The favored local geometry was conclusively shown to have nearly a tetrahedron structure with consequences for a sp^3 hybridization.

In order to study the bonding via the amino group, we have dropped the activity of the thiol group and studied the adsorption of the smaller amino-acid-molecule glycine. We found an off-top position of the N atom of the amino group as the most-favored adsorption site. However, the precise bonding geometry was less important, indicating a flexibility of the amino-Au bond. The studies of the charge redistribution revealed similarities to the amino bonding on the Cu(110) surface. The bond was shown to be largely electrostatic and multipole terms beyond the ionic attraction seem to play a considerable role. The filling and energetics of N electronic states have been shown to be important for the bonding behavior. For instance, the adsorption-induced charge transfer was shown to be due to interaction of the N-localized glycine HOMO state with the Au *d* bands. The electron transfer from molecule to surface caused a potential shift in the area of the amino group, thus shifting amino-localized states to lower energies.

The knowledge of the properties of isolated N-Au and S-Au bonds has been used to find the optimum adsorbate geometry. Thereby, the registering of the molecule on the metal surface, i.e., steric effects, and subsequent deformations of the molecules were investigated. The geometries for which low adsorption energies have been estimated correspond to flat adsorption configurations with different N and S adsorption sites. For comparison one upright adsorption-geometry docking to the surface solely via the thiol head group was studied as well. Flat molecular adsorption geometries proved to be energetically favored over upright configurations, taking advantage of both the thiolate and the amino-Au bond. The choice of the $[1\bar{1}0]$ bridge site as favored bonding site for the sulfur head group in flat adsorption configurations has been supported by studies of other groups. Molecular adsorption was discussed in terms of electron redistribution, changes in the site-projected density of states and adsorption-induced surface rearrangements. The combined characteristics of amino-Au and thiolate-Au bonds were present in the respective aspects of the adsorbed systems. The observed dominant role of the thiolate bond is supported by the fact that the adsorption configuration with optimum thiolate-bond site was determined to be energetically most favorable despite the fact that the amino-Au bond was weaker and the adsorption-induced strain in the substrate larger than for the other flat adsorption configurations.

Since the adsorption process is largely dominated by the thiolate bond, the preference of flat adsorption configurations might not hold for all surface orientations and metals with filled *d* shells. Since the binding energy of the thiolate bond proved to be very sensitive to changes in the bonding geometry, the preference for a flat adsorption geometry depends on the formation of amino (or other) bonds while retaining the favored tetrahedronlike geometry of the thiolate bond, i.e., it depends on surface structure and lattice constant of the substrate.

Our results should also be relevant for the investigation of self-assembled cysteine monolayers, dimer-adsorption, and other higher coverage structures. In the case of complex biomolecules attached to metallic supports through cysteine residues, the discussed flat adsorption configurations and energies might be of limited value, since in those systems the NH_2 group is usually engaged in peptide bonds along the primary chain. For future investigations of such systems, the results concerning the upright adsorption configuration should be of interest. Since the influence of the molecular tail on the properties of the single bonds proved to be small, the results obtained by the detailed analysis of S-Au and N-Au bonds should be applicable for other problems such as the adsorption of nucleobases or alkanethiols. In particular, the influence of the bonding geometry on metal-thiolate bonds could be exploited on a larger scale, as in the usage of cysteine as an anchoring group for functional biomolecular structures.

ACKNOWLEDGMENTS

Useful discussions with M. Preuss and J. Furthmüller are acknowledged. We would like to thank the Deutsche Forschungsgemeinschaft (Project No. HA 2900/3-2,3) and the BMBF (Contract No. 13N9689) for financial support. The research was also funded by the European Community within the framework of ETSF (Grant No. 211956). We thank the Höchstleistungsrechenzentrum Stuttgart and the Leibniz-Rechenzentrum München for granted computer time.

[1] A. Nilsson and G. M. Petterson, Surf. Sci. Rep. **55**, 49 (2004).
[2] H. Ishii, K. Sugiyama, I. Eisuke, and K. Seki, Adv. Mater. (Weinheim, Ger.) **11**, 605 (1999).
[3] G. Heimel, L. Romaner, J.-L. Brédas, and E. Zojer, Phys. Rev. Lett. **96**, 196806 (2006).
[4] H. Vázquez, Y. J. Dappe, J. Ortega, and F. Flores, J. Chem. Phys. **126**, 144703 (2007).
[5] I. G. Hill, A. Rajagopal, A. Kahn, and Y. Hu, Appl. Phys. Lett. **73**, 662 (1998).
[6] W. G. Schmidt, K. Seino, M. Preuss, A. Hermann, F. Ortmann, and F. Bechstedt, Appl. Phys. A: Mater. Sci. Process. **85**, 387 (2006).
[7] C. Vericat, M. E. Vela, and R. C. Salvarezza, Phys. Chem. Chem. Phys. **7**, 3258 (2005).
[8] V. De Renzi, R. Rousseau, D. Marchetto, R. Biagi, S. Scandolo, and U. del Pennino, Phys. Rev. Lett. **95**, 046804 (2005).
[9] E. Rauls, S. Blankenburg, and W. G. Schmidt, Surf. Sci. **602**, 2170 (2008).
[10] A. Bilić, J. R. Reimer, N. S. Hush, and J. Hafner, J. Chem. Phys. **116**, 8981 (2002).
[11] C. Joachim, J. K. Gimzewski, and A. Aviram, Nature (London) **408**, 541 (2000).
[12] H. B. Akkerman, P. W. M. Blom, D. M. de Leeuw, and B. de Boer, Nature (London) **441**, 69 (2006).
[13] C. P. Collier, E. W. Wong, M. Belohradsky, F. M. Raymo, J. F. Stoddart, P. J. Kuekes, R. S. Williams, and J. R. Heath, Science **285**, 391 (1999).
[14] M. Reed, C. Zhou, C. J. Muller, T. P. Burgin, and J. M. Tour, Science **278**, 252 (1997).
[15] S. Y. Quek, L. Venkataraman, H. J. Choi, S. G. Louie, M. S. Hybertsen, and J. B. Neaton, Nano Lett. **7**, 3477 (2007).
[16] J. Zhang, Q. Chi, J. U. Nielsen, E. P. Friis, J. E. T. Andersen, and J. Ulstrup, Langmuir **16**, 7229 (2000).
[17] R. R. Nazmutdinov, J. D. Zhang, T. T. Zinkicheva, I. R. Manyurov, and J. Ulstrup, Langmuir **22**, 7556 (2006).
[18] A. Kühnle, T. R. Linderoth, M. Schunack, and F. Besenbacher, Langmuir **22**, 2156 (2006).
[19] A. Kühnle, T. R. Linderoth, B. Hammer, and F. Besenbacher, Nature (London) **415**, 891 (2002).
[20] A. Kühnle, L. M. Molina, T. R. Linderoth, B. Hammer, and F. Besenbacher, Phys. Rev. Lett. **93**, 086101 (2004).
[21] A. Kühnle, T. R. Linderoth, and F. Besenbacher, J. Am. Chem. Soc. **128**, 1076 (2006).
[22] A. Kühnle, T. R. Linderoth, and F. Besenbacher, J. Am. Chem. Soc. **125**, 14680 (2003).
[23] T. Greber, Ž. Šljivančanin, R. Schillinger, J. Wider, and B. Hammer, Phys. Rev. Lett. **96**, 056103 (2006).
[24] R. Schillinger, Z. Sljivancanin, B. Hammer, and T. Greber, Phys. Rev. Lett. **98**, 136102 (2007).
[25] B. Höffling, F. Ortmann, K. Hannewald, and F. Bechstedt, Phys. Status Solidi C (to be published).
[26] R. Di Felice, A. Selloni, and E. Molinari, J. Phys. Chem. B **107**, 1151 (2003).
[27] R. Di Felice and A. Selloni, J. Chem. Phys. **120**, 4906 (2004).
[28] J. P. Perdew, *Electronic Structure of Solids '91* (Akademie-Verlag, Berlin, 1991), p. 11.
[29] J. P. Perdew and Y. Wang, Phys. Rev. B **45**, 13244 (1992).
[30] R. Maul, M. Preuss, F. Ortmann, K. Hannewald, and F. Bechstedt, J. Phys. Chem. A **111**, 4370 (2007).
[31] G. Kresse and D. Joubert, Phys. Rev. B **59**, 1758 (1999).
[32] R. Maul, F. Ortmann, M. Preuss, K. Hannewald, and F. Bechstedt, J. Comput. Chem. **28**, 1817 (2007).
[33] M. Preuss, W. G. Schmidt, K. Seino, J. Furthmüller, and F. Bechstedt, J. Comput. Chem. **25**, 112 (2004).
[34] H. J. Monkhorst and J. D. Pack, Phys. Rev. B **13**, 5188 (1976).
[35] G. Kresse and J. Furthmüller, Comput. Mater. Sci. **6**, 15 (1996).
[36] M. Preuss and F. Bechstedt, Surf. Sci. **602**, 1643 (2008).
[37] A. Y. Lozovoi and A. Alavi, Phys. Rev. B **68**, 245416 (2003).
[38] S. D'Agostino, L. Chiodo, F. Della Sala, R. Cingolani, and R. Rinaldi, Phys. Rev. B **75**, 195444 (2007).
[39] Sargent-Welch, *Table of Periodic Properties of the Elements* (Sargent-Welch Scientific Company, Skokie, IL, 1980).
[40] A. Bilić, J. R. Reimers, and N. S. Hush, J. Chem. Phys. **122**, 094708 (2005).
[41] S. Blankenburg and W. G. Schmidt, Phys. Rev. Lett. **99**, 196107 (2007).
[42] W. G. Aulbur, L. Jonsson, and J. W. Wilkins, Solid State Phys. **54**, 1 (2000).
[43] M. Preuss, W. G. Schmidt, and F. Bechstedt, Phys. Rev. Lett. **94**, 236102 (2005).
[44] F. Ortmann, W. G. Schmidt, and F. Bechstedt, Phys. Rev. Lett. **95**, 186101 (2005).
[45] The initial configuration had S at the $[1\bar{1}0]$ off-bridge site, the thiol side group moved during the ionic relaxation due to intramolecular strain caused by the pull of the amino-Au bond.
[46] G. R. Desiraju and T. Steiner, *The Weak Hydrogen Bond in Structural Chemistry and Biology* (Oxford University Press, Oxford, 1999).
[47] N. N. Greenwood and A. Earnshaw, *Chemie der Elemente* (VCH, Weinheim, 1988).